




 Cite this: *Chem. Commun.*, 2024, 60, 10204

 Received 17th June 2024,  
 Accepted 22nd August 2024

DOI: 10.1039/d4cc02928c

rsc.li/chemcomm

# Enhancing CO<sub>2</sub> electroreduction to ethylene via microenvironment regulation in boron–imidazolate frameworks†

 Chen Lu,<sup>ab</sup> Qin-Long Hong,<sup>a</sup> Hai-Xia Zhang \*<sup>a</sup> and Jian Zhang \*<sup>a</sup>

Using the structure-induced effect of KBH(mim)<sub>3</sub> ligand, four 2-dimensional (2D) boron imidazolate frameworks with identical body framework and different dangling monocarboxylate ligands, have been synthesized. Electrocatalytic results indicate that the surrounding microenvironment regulation could effectively affect the activity and selectivity towards C<sub>2</sub>H<sub>4</sub>. BIF-151 showed the highest electrocatalytic performances with the Faraday efficiency (FE) of 25.94% for C<sub>2</sub>H<sub>4</sub> at –1.4 V vs. RHE.

With the rapid development of modern society and the extensive consumption of non-renewable fossil fuels, significant amounts of CO<sub>2</sub> gas are being emitted into the atmosphere, resulting in a profound impact on Earth's ecological environment.<sup>1–4</sup> Electrochemical CO<sub>2</sub> reduction reaction (CO<sub>2</sub>RR) is a process that utilizes electrical energy to expedite the conversion of CO<sub>2</sub> on electrode surfaces into carbon products such as CO, CH<sub>4</sub>, etc.<sup>5–12</sup> This process not only serves as an important approach to address energy issues and achieve carbon-neutral recycling but also plays a crucial role in laboratory investigations regarding CO<sub>2</sub> reduction.<sup>13–16</sup> Through relentless efforts by scientific researchers, the range of products obtained from CO<sub>2</sub>RR has gradually expanded from single-carbon compounds like CO and CH<sub>4</sub> to multi-carbon compounds including ethylene (C<sub>2</sub>H<sub>4</sub>) and ethanol (C<sub>2</sub>H<sub>5</sub>OH).<sup>17–20</sup> Among these various carbon products, C<sub>2</sub>H<sub>4</sub> possesses high energy density and holds immense economic significance.<sup>21–23</sup> However, due to the sluggish kinetics associated with carbon–carbon (C–C) coupling reactions during this process, achieving selective conversion of CO<sub>2</sub> into C<sub>2</sub>H<sub>4</sub> remains a major challenge.<sup>24–27</sup>

Being used as electrocatalysts, crystalline boron imidazolate frameworks (BIFs) have achieved excellent results in the study

of electrocatalytic performance–structure relationship.<sup>28–30</sup> At present, the reported BIFs catalysts mainly focus on the design of active metal sites (bimetal, monometallic sites) and tandem catalysis by anchoring second active metal sites.<sup>31–33</sup> Except for metal sites, the effects of surrounding ligand microenvironment on electrocatalytic activity and selectivity have been poorly studied.<sup>34–36</sup> During the process of CO<sub>2</sub>RR to C<sub>2</sub>H<sub>4</sub>, C–C coupling is the indispensable step which require synergistic effect of multiple sites, including metal sites and organic ligands.<sup>37–39</sup> In order to strictly compare the effects of the ligand microenvironment on catalysis, the synthesized catalyst should be constructed from different functional ligands while contain the same metal species, identical metal coordination environment, even exhibit similar topological structures. However, in the synthesis process of crystalline catalysts, small changes in the synthesis conditions (temperature, solvent, pH, etc.) and raw materials will significantly affect the structures of the resulting products. Therefore, to discern the contributions of diverse surrounding ligand microenvironment, it is necessary to construct a stable metal–organic skeleton platform with the same topology, so as to fix the coordination environment of host framework and change the functional ligand systematically.

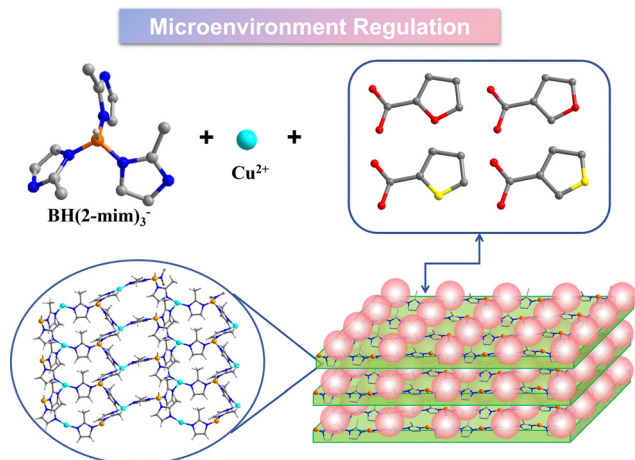
Herein, a series of isostructural 2D BIFs, Cu(II)<sub>2</sub>[BH(mim)<sub>3</sub>]<sub>2</sub>(2-FC) (BIF-151, mim = 2-methylimidazole, 2-FC = furan-2-carboxylate), Cu(II)<sub>2</sub>[BH(mim)<sub>3</sub>]<sub>2</sub>(3-FC) (BIF-152, 3-FC = furan-3-carboxylate), Cu(II)<sub>2</sub>[BH(mim)<sub>3</sub>]<sub>2</sub>(2-TpC) (BIF-153, 2-TpC = thiophene-2-carboxylate) and Cu(II)<sub>2</sub>[BH(mim)<sub>3</sub>]<sub>2</sub>(3-TpC) (BIF-154, 3-TpC = thiophene-3-carboxylate) were successfully constructed under solvothermal condition (Scheme 1). Thanks to the structure-induced effect of KBH(mim)<sub>3</sub> ligand, these crystal structures exhibited identical body framework and metal coordination environment. While, four types of monocarboxylate ligands with different substituent elements and substituent positions could be used as dangling ligands to modify these layers. Electrocatalytic results indicate that all four materials demonstrate catalytic activity towards CO<sub>2</sub>RR, especially with certain selectivity towards C<sub>2</sub>H<sub>4</sub> products. However, the activity and selectivity towards C<sub>2</sub>H<sub>4</sub> were distinctly different. Among them, BIF-151

<sup>a</sup> State Key Laboratory of Structural Chemistry, Fujian Institute of Research on the Structure of Matter, Chinese Academy of Sciences, Fuzhou, Fujian 350002, P. R. China. E-mail: zhanghaixia@fjirsm.ac.cn, zhj@fjirsm.ac.cn

<sup>b</sup> University of Chinese Academy of Sciences, Beijing 100049, P. R. China

† Electronic supplementary information (ESI) available: TGA diagram, powder X-ray diffraction, CD, UV, etc. Crystal data and structure refinement details. CCDC 2362473–2362476. For ESI and crystallographic data in CIF or other electronic format see DOI: <https://doi.org/10.1039/d4cc02928c>





**Scheme 1** Synthesis procedure and the layer structure diagram. The pink sphere denotes the second ligand and the light green lamellar represents  $\text{CuBH(mim)}_3^+$  layer.

showed the highest electrocatalytic performances with the FE of 25.94% for  $\text{C}_2\text{H}_4$  at  $-1.4$  V vs. RHE, which is about 1.9, 1.7, and 2.8 times higher than that of BIF-152 (13.04%), BIF-153 (15.05%), and BIF-154 (9.26%), respectively.

Firstly, tripodal boron imidazolate ligands ( $\text{KBH(mim)}_3$ ) were synthesized prior to the solvothermal reaction. The tripodal  $\text{KBH(mim)}_3$  ligands can induce 3-connected copper sites during the self-assembly process. By adopting a variety of dangling monocarboxylate ligands, four 3-connected layer structures have been obtained (BIF-151 to BIF-154). X-ray single-crystal structure tests revealed that the four structures have almost identical framework, which all crystallized in the monoclinic space group *Ia*. Since they are isomorphic, BIF-151 is selected to describe their structures. The asymmetric unit of BIF-151 includes one crystallographically independent  $\text{Cu(II)}$  ion, one  $\text{BH(mim)}_3^-$  ligand and one furan-2-carboxylate ligand. As shown in Fig. 1a, each  $\text{Cu(II)}$  ion adopted a pentadentate triangular dipyramidal coordination pattern, wherein three N atoms originate from three  $\text{BH(mim)}_3^-$  ligands and two O atoms derive from carboxyl group of furan-2-carboxylate. Each  $\text{BH(mim)}_3^-$  ligand adopted the  $\mu_3$ -bridged mode linking three copper ions. Thus,  $\text{Cu(II)}$  ions and B atoms are alternately linked *via* mim ligands to generate a 2D honeycomb layer (Fig. 1b). These 2D layers stack along the *c*-axis direction through van der Waals interactions (Fig. 1c and e), while maintaining a certain distance between them due to the presence of dangling monocarboxylate ligands on one side of each layer.

The 3-connected layer structures can be constructed precisely due to the structural induction of the tripodal  $\text{BH(mim)}_3^-$  ligands. Therefore, we can fix the coordination environment of copper ions and micro-regulate the surrounding environment by changing the dangling monocarboxylate ligands. The position of oxygen on furan can be changed. BIF-152 ( $\text{CuBH(mim)}_3(3\text{-FC})$ ) was synthesized when furan-3-carboxylate ligand is used instead of furan-2-carboxylate ligand (Fig. S1, ESI<sup>†</sup>). Furtherly, thiophene-2-carboxylate and thiophene-3-carboxylate ligands can be applied in the similar

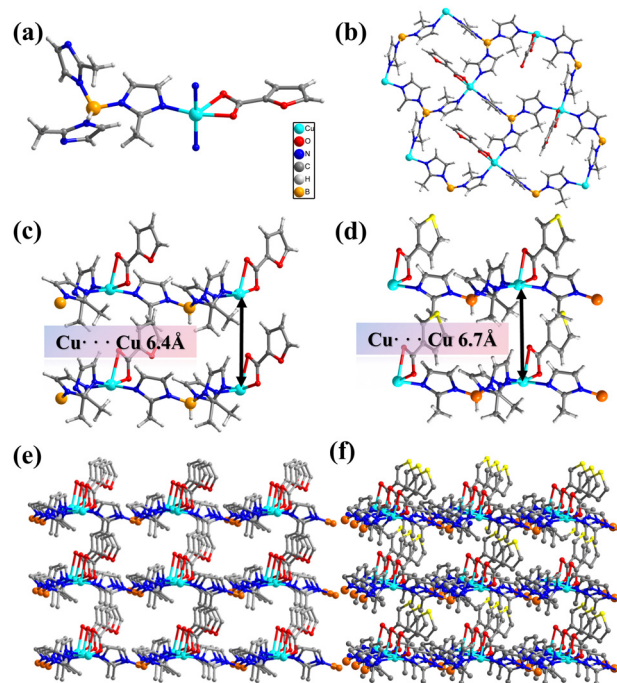


**Fig. 1** (a) Coordination environment of BIF-151; (b) the 2D layer structure of BIF-151; the  $\text{Cu}\cdots\text{Cu}$  distance between adjacent layer of (c) BIF-151 and (d) BIF-154; the 3D stacking model of (e) BIF-151 and (f) BIF-154.

synthetic reaction and two new crystals BIF-153 ( $\text{CuBH(mim)}_3(2\text{-TpC})$ ) (Fig. S1, ESI<sup>†</sup>) and BIF-154 ( $\text{CuBH(mim)}_3(3\text{-TpC})$ ) (Fig. 1d and f) were constructed. Specifically, when thiophene carboxylate ligand serves as the second ligand, the spacing between layers was measured at 6.7 Å; whereas when furan carboxylate ligand acts as the second ligand, this spacing reduced to 6.4 Å. The presence of interspaces reduces the weak interactions between layers and may contribute to the intercalation of small molecules.

The powder X-ray diffraction (PXRD) patterns were performed to investigate the stability and crystal purity of these crystals. As shown in Fig. 2 and Fig. S2 (ESI<sup>†</sup>), the synthesized crystal samples have high purity, and the positions of the diffraction peaks of the crystals are basically consistent with the simulated characteristic peaks. By immersing the crystal samples in aqueous solutions with different pH values (using dilute nitric acid or sodium hydroxide to adjust the pH) for 3 days, the diffraction peaks were maintained, demonstrating the chemical stability of these crystals (Fig. S3, ESI<sup>†</sup>). In addition,

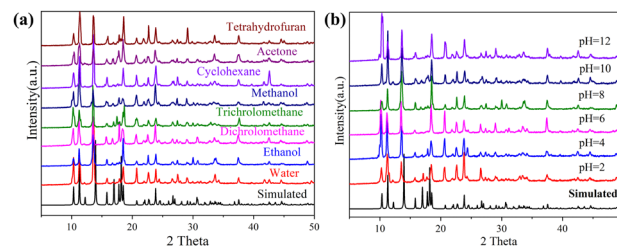


**Fig. 2** The powder XRD patterns of BIF-151: (a) solvent stability and (b) chemical stability.



the crystal samples were stable and insoluble in common solvents, such as water, dichloromethane, tetrahydrofuran, methanol, ethanol, trichloromethane and acetone (Fig. S4, ESI<sup>†</sup>). The chemical composition and valence state were studied by X-ray photoelectron spectroscopy (Fig. S6, ESI<sup>†</sup>). The XPS survey scans displayed the presence of carbon, nitrogen, oxygen, copper and boron in these materials. High-resolution spectra of the Cu 2p region of BIF-151 showed that there are only bivalent copper ions in these crystal structures, and the fitting peaks at 954.2 eV and 934.2 eV correspond to the binding energies of the Cu 2p 1/2 and Cu 2p 3/2 orbitals, respectively. The XPS spectra of crystals BIF-152, BIF-153, and BIF-154 were similar to the above (Fig. S6, ESI<sup>†</sup>), demonstrating that the peripheral groups have little effect on the valence state of copper.

To study the effect of different organic modifications on catalytic activity, the four BIFs were used as catalysts for electrochemical CO<sub>2</sub> reduction reaction. The electrocatalytic activity was measured in 0.05 M CsCO<sub>3</sub> and 0.1 M KCl (v:v = 1:1) solution saturated with CO<sub>2</sub> from 0 to -1.6 V vs. reversible hydrogen electrode (RHE). On the base of linear sweep voltammetry (LSV), BIF-151 displayed the most positive onset potential of -0.37 V vs. RHE and the highest total current density at potential from -0.6 V to -1.6 V vs. RHE when comparing with other crystals (Fig. 3a). The potential gradient and the FE of each product were measured at constant potential. The gas phase products and liquid phase products were detected by gas chromatography (GC) and ion chromatography (IC), respectively. The main gas products included CO, CH<sub>4</sub> and C<sub>2</sub>H<sub>4</sub>, and the liquid product was HCOOH. As shown in Fig. 3b and Fig. S8 (ESI<sup>†</sup>), the FEs of each product strictly depended on the working potential. For BIF-151 (Fig. 3b), the highest FE (32.53%) for HCOOH was detected at the lowest potential. With the negative shifting of potential, FE<sub>HCOOH</sub>

decreased gradually while C<sub>2</sub>H<sub>4</sub> became the dominant product of CO<sub>2</sub> reduction. The FEs for C<sub>2</sub>H<sub>4</sub> increased with the potential shifted from -1.2 V to -1.4 V and reached the maximum value of 25.94% at -1.4 V, which is much higher than that of CO, CH<sub>4</sub>. Meanwhile, the high FE<sub>C<sub>2</sub>H<sub>4</sub></sub> (about 20%) of BIF-151 can be maintained in a potential range of -1.2 V to -1.6 V, indicating the good selectivity of BIF-151 for C<sub>2</sub> products. The other three catalysts (BIF-152, 153 and 154) showed the similar product distributions as BIF-151, but were much less active for C<sub>2</sub>H<sub>4</sub> (Fig. 3c). With the same substituted position (2-substituted) as that of BIF-151, BIF-153 was the second active catalyst with a highest FE<sub>C<sub>2</sub>H<sub>4</sub></sub> of 16.67%. In comparison, the 3-substituted two catalysts, BIF-152 and 154 exhibited much lower selectivity for C<sub>2</sub>H<sub>4</sub>, with the highest FEs<sub>C<sub>2</sub>H<sub>4</sub></sub> of 13.04% and 9.99%, respectively. Correspondingly, electrochemical double-layer capacitances (C<sub>dl</sub>) are calculated from cyclic voltammetry (CV) curves to estimate the electrochemical active surface area (Fig. 3d and Fig. S9, ESI<sup>†</sup>). BIF-151 exhibited the largest C<sub>dl</sub> value (3.80 mF cm<sup>-2</sup>) than those of BIF-152 (3.50 mF cm<sup>-2</sup>), BIF-153 (3.48 mF cm<sup>-2</sup>) and BIF-154 (2.90 mF cm<sup>-2</sup>), basically consistent with the results of electrochemical tests. Given the identical metal coordination environment of the four catalysts, the distinctly different performance between them revealed that the catalytic activity and selectivity are not only strongly dependent on active metal sites, but also influenced by surrounding ligand environment, such as the composition and position of the substituent elements, *etc.*

In this work, we successfully constructed a stable metal boron imidazolate skeleton platform with the 2D topology by the structure-induced effect of KBH(mim)<sub>3</sub> ligand. Moreover, the surrounding microenvironments of these 2D layers can be adjusted by a series of dangling monocarboxylate ligands with different substituent elements and substituent positions. Electrocatalytic performance results indicate that all these materials demonstrate catalytic activity towards CO<sub>2</sub>RR, especially with certain selectivity towards C<sub>2</sub>H<sub>4</sub> products. However, the activity and selectivity towards C<sub>2</sub>H<sub>4</sub> were distinctly different. Among them, BIF-151 showed the highest electrocatalytic performances with the FE of 25.94% for C<sub>2</sub>H<sub>4</sub> at -1.4 V vs. RHE, which is about 1.9, 1.7, and 2.8 times higher than that of BIF-152 (13.04%), BIF-153 (15.05%), and BIF-154 (9.26%), respectively.

This work was supported by National Key Research and Development Program of China (2021YFA1501500), National Natural Science Foundation of China (22275192), the STS Project of Fujian-CAS (Grant No. 2023T3054).

## Data availability

The data supporting this article have been included as part of the ESI.<sup>†</sup>

## Conflicts of interest

There are no conflicts to declare.

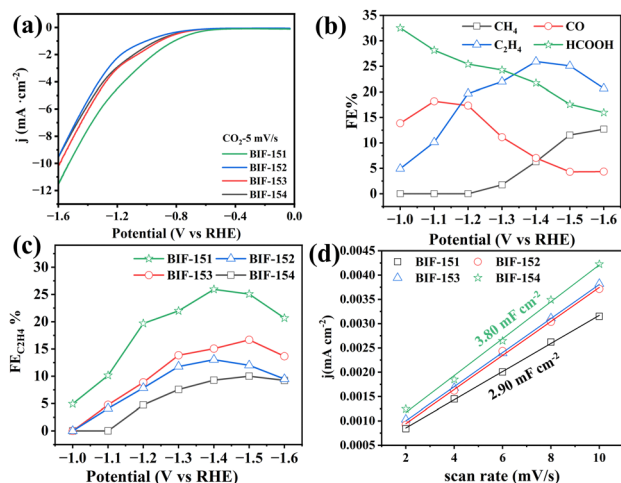


Fig. 3 (a) LSV curves of BIF-151, BIF-152, BIF-153 and BIF-154 electrocatalysts in CO<sub>2</sub> saturated 0.5 M KHCO<sub>3</sub> electrolyte, respectively; (b) the FE of gas products and liquid products of BIF-151 electrocatalyst at different applied potentials in CO<sub>2</sub> saturated electrolyte; (c) the FE<sub>C<sub>2</sub>H<sub>4</sub></sub> of BIF-151, BIF-152, BIF-153, and BIF-154 electrocatalyst; (d) the C<sub>dl</sub> of BIF-151, BIF-152, BIF-153, and BIF-154 electrocatalyst.



## Notes and references

- 1 K. Caldeira, A. K. Jain and M. I. Hoffert, *Science*, 2003, **299**, 2052–2054.
- 2 K. S. Novoselov, A. K. Geim, S. V. Morozov, D. Jiang, Y. Zhang, S. V. Dubonos, I. V. Grigorieva and A. A. Firsov, *Science*, 2004, **306**, 666–669.
- 3 V. Humphrey, J. Zscheischler, P. Ciaia, L. Gudmundsson, S. Sitch and S. I. Seneviratne, *Nature*, 2018, **560**, 628–631.
- 4 S. I. Seneviratne, M. G. Donat, A. J. Pitman, R. Knutti and R. L. Wilby, *Nature*, 2016, **529**, 477–483.
- 5 A. R. Woldu, Z. Huang, P. Zhao, L. Hu and D. Astruc, *Coord. Chem. Rev.*, 2022, **454**, 214340.
- 6 C. Cong and H. Ma, *Small*, 2023, **19**, 2207547.
- 7 C. Zhao, X. Dai, T. Yao, W. Chen, X. Wang, J. Wang, J. Yang, S. Wei, Y. Wu and Y. Li, *J. Am. Chem. Soc.*, 2017, **139**, 8078–8081.
- 8 Y. Guo, H. Yang, X. Zhou, K. Liu, C. Zhang, Z. Zhou, C. Wang and W. Lin, *J. Mater. Chem. A*, 2017, **5**, 24867–24873.
- 9 Z. Xu, Y. Xie and Y. Wang, *Mater. Rep.: Energy*, 2023, **3**, 100173.
- 10 J. Jin, G. Cao, Y. Liu, Y. Shu, Z. Deng, W. Sun and X. Yang, *Mater. Rep.: Energy*, 2023, **3**, 100229.
- 11 B. Xu, I. M. U. Hasan, L. Peng, J. Liu, N. Xu, M. Fan, N. K. Niazi and J. Qiao, *Mater. Rep.: Energy*, 2022, **2**, 100139.
- 12 Z.-N. Wei, M.-N. Cao and R. Cao, *J. Electrochem.*, 2022, 2215008.
- 13 Y. Y. Birdja, E. Pérez-Gallent, M. C. Figueiredo, A. J. Göttle, F. Calle-Vallejo and M. T. M. Koper, *Nat. Energy*, 2019, **4**, 732–745.
- 14 N. Kornienko, Y. B. Zhao, C. S. Kiley, C. H. Zhu, D. Kim, S. Lin, C. J. Chang, O. M. Yaghi and P. D. Yang, *J. Am. Chem. Soc.*, 2015, **137**, 14129–14135.
- 15 S. Jin, Z. M. Hao, K. Zhang, Z. H. Yan and J. Chen, *Angew. Chem., Int. Ed.*, 2021, **60**, 20627–20648.
- 16 Z.-H. Zhao, K. Zheng, N.-Y. Huang, H.-L. Zhu, J.-R. Huang, P.-Q. Liao and X.-M. Chen, *Chem. Commun.*, 2021, **57**, 12764–12767.
- 17 H. B. Yang, S. F. Hung, S. Liu, K. D. Yuan, S. Miao, L. P. Zhang, X. Huang, H. Y. Wang, W. Z. Cai, R. Chen, J. J. Gao, X. F. Yang, W. Chen, Y. Q. Huang, H. M. Chen, C. M. Li, T. Zhang and B. Liu, *Nat. Energy*, 2018, **3**, 140–147.
- 18 K. P. Kuhl, T. Hatsukade, E. R. Cave, D. N. Abram, J. Kibsgaard and T. F. Jaramillo, *J. Am. Chem. Soc.*, 2014, **136**, 14107–14113.
- 19 H. Song, M. Im, J. T. Song, J. A. Lim, B. S. Kim, Y. Kwon, S. Ryu and J. Oh, *Appl. Catal., B*, 2018, **232**, 391–396.
- 20 Y. Li, S. L. Zhang, W. Cheng, Y. Chen, D. Luan, S. Gao and X. W. Lou, *Adv. Mater.*, 2022, **34**, 2105204.
- 21 C. Kong, G. Jiang, Y. Sheng, Y. Liu, F. Gao, F. Liu and X. Duan, *Chem. Eng. J.*, 2023, **460**, 141803.
- 22 C. T. Dinh, T. Burdyny, M. G. Kibria, A. Seifitokaldani, C. M. Gabardo, F. P. G. de Arquer, A. Kiani, J. P. Edwards, P. De Luna, O. S. Bushuyev, C. Q. Zou, R. Quintero-Bermudez, Y. J. Pang, D. Sinton and E. H. Sargent, *Science*, 2018, **360**, 783–787.
- 23 T. Yan, X. Chen, L. Kumari, J. Lin, M. Li, Q. Fan, H. Chi, T. J. Meyer, S. Zhang and X. Ma, *Chem. Rev.*, 2023, **123**, 10530–10583.
- 24 S. Nitopi, E. Bertheussen, S. B. Scott, X. Y. Liu, A. K. Engstfeld, S. Horch, B. Seger, I. E. L. Stephens, K. Chan, C. Hahn, J. K. Nørskov, T. F. Jaramillo and I. Chorkendorff, *Chem. Rev.*, 2019, **119**, 7610–7672.
- 25 Y. Zheng, A. Vasileff, X. L. Zhou, Y. Jiao, M. Jaroniec and S. Z. Qiao, *J. Am. Chem. Soc.*, 2019, **141**, 7646–7659.
- 26 G. L. De Gregorio, T. Burdyny, A. Loudice, P. Iyengar, W. A. Smith and R. Buonsanti, *ACS Catal.*, 2020, **10**, 4854–4862.
- 27 F. Chang, M. Xiao, R. Miao, Y. Liu, M. Ren, Z. Jia, D. Han, Y. Yuan, Z. Bai and L. Yang, *Electrochem. Energy Rev.*, 2022, **5**, 4.
- 28 H.-X. Zhang, C. Lu and J. Zhang, *Acc. Mater. Res.*, 2023, **4**, 995–1007.
- 29 G. Xu, Q.-L. Hong, Y. Sun, M. Liu, H.-X. Zhang and J. Zhang, *Chin. Chem. Lett.*, 2022, **33**, 2915–2918.
- 30 Z.-Y. Chen, Q.-L. Hong, H.-X. Zhang and J. Zhang, *ACS Appl. Energy Mater.*, 2022, **5**, 1175–1182.
- 31 P. Shao, Y.-M. Wan, L. Yi, S. Chen, H.-X. Zhang and J. Zhang, *Small*, 2024, **20**, 2305199.
- 32 C. S. Gerke, Y. Xu, Y. Yang, G. D. Foley, B. Zhang, E. Shi, N. M. Bedford, F. Che and V. S. Thoi, *J. Am. Chem. Soc.*, 2023, **145**, 26144–26151.
- 33 P. Shao, W. Zhou, Q.-L. Hong, L. Yi, L. Zheng, W. Wang, H.-X. Zhang, H. Zhang and J. Zhang, *Angew. Chem., Int. Ed.*, 2021, **60**, 16687–16692.
- 34 Y. Zhang, Q. Zhou, Z.-F. Qiu, X.-Y. Zhang, J.-Q. Chen, Y. Zhao, F. Gong and W.-Y. Sun, *Adv. Funct. Mater.*, 2022, **32**, 2203677.
- 35 H. Li, J. Zhao, L. Luo, J. Du and J. Zeng, *Acc. Chem. Res.*, 2021, **54**, 1454–1464.
- 36 L. Jiao, J. Wang and H.-L. Jiang, *Acc. Mater. Res.*, 2021, **2**, 327–339.
- 37 J. H. Montoya, C. Shi, K. Chan and J. K. Nørskov, *J. Phys. Chem. Lett.*, 2015, **6**, 2032–2037.
- 38 D. Cheng, Z.-J. Zhao, G. Zhang, P. Yang, L. Li, H. Gao, S. Liu, X. Chang, S. Chen, T. Wang, G. A. Ozin, Z. Liu and J. Gong, *Nat. Commun.*, 2021, **12**, 395.
- 39 R. Kortlever, J. Shen, K. J. P. Schouten, F. Calle-Vallejo and M. T. M. Koper, *J. Phys. Chem. Lett.*, 2015, **6**, 4073–4082.

